Unveiling a phytoplankton hotspot at a narrow boundary between coastal and offshore waters

Francois Ribalet[a], Adrian Marchetti[a], Katherine A. Hubbard[a], Kristina Brown[b], Colleen A. Durkin[a], Rhonda Morales[a], Marie Robert[c], Jarred E. Swalwell[a], Philippe D. Tortell[b], and E. Virginia Armbrust[a,1]

[a]School of Oceanography, University of Washington, Seattle, WA, 98195; [b]Department of Earth and Ocean Sciences and Department of Botany, University of British Columbia, Vancouver, BC, Canada V6T 1Z4; and [c]Fisheries and Oceans Canada, Institute of Ocean Sciences, Sidney, BC, Canada V8L 4B2

Edited by David M. Karl, University of Hawaii, Honolulu, HI, and approved August 17, 2010 (received for review May 3, 2010)

In terrestrial ecosystems, transitional areas between different plant communities (ecotones) are formed by steep environmental gradients and are commonly characterized by high species diversity and primary productivity, which in turn influences the foodweb structure of these regions. Whether comparable zones of elevated diversity and productivity characterize ecotones in the oceans remains poorly understood. Here we describe a previously hidden hotspot of phytoplankton diversity and productivity in a narrow but seasonally persistent transition zone at the intersection of iron-poor, nitrate-rich offshore waters and iron-rich, nitrate-poor coastal waters of the Northeast Pacific Ocean. Novel continuous measurements of phytoplankton cell abundance and composition identified a complex succession of blooms of five distinct size classes of phytoplankton populations within a 100-km–wide transition zone. The blooms appear to be fueled by natural iron enrichment of offshore communities as they are transported toward the coast. The observed succession of phytoplankton populations is likely driven by spatial gradients in iron availability or time since iron enrichment. Regardless of the underlying mechanism, the resulting communities have a strong impact on the regional biogeochemistry as evidenced by the low partial pressure of CO_2 and the nearly complete depletion of nutrients. Enhanced phytoplankton productivity and diversity associated with steep environmental gradients are expected wherever water masses with complementary nutrient compositions mix to create a region more favorable for phytoplankton growth. The ability to detect and track these important but poorly characterized marine ecotones is critical for understanding their impact on productivity and ecosystem structure in the oceans.

ecotone | transition zone | iron | high-nitrate, low-chlorophyll | flow cytometry

The surface ocean is characterized by steep gradients in density, which limit the mixing of different water types. These physical boundaries also separate the associated phytoplankton communities, potentially creating marine transition zones (1) comparable to the physically mediated transitions between terrestrial plant communities (2). Distinctive plant communities often thrive within the terrestrial transition zones, resulting in enhanced species diversity and productivity within these specialized regions known as ecotones (3). A high diversity of marine phytoplankton species (4) and, in some cases, high productivity (5–8) are associated with regions of intense ocean circulation and physical fronts. Comparable marine ecotones are expected throughout the world's oceans wherever density gradients demarcate water masses with complementary nutrient compositions. Mixing of these water types can create more favorable nutrient conditions within the transition zone that will enhance phytoplankton biomass and productivity. What remains unclear is whether distinctive phytoplankton communities exist within these transition zones and the potential influence of these communities on surface ocean biogeochemical cycles.

The North Pacific Ocean is among the most productive marine ecosystems and one of the largest sinks of atmospheric CO_2 in the world's oceans (9). The eastern part of the North Pacific Ocean offshore waters is characterized by a vast gyre that is a high-nitrate, low-chlorophyll (HNLC) region where phytoplankton productivity is limited by the availability of iron (10, 11). The resulting low-biomass phytoplankton assemblage is dominated by small-celled phytoplankton, such as the cyanobacteria *Synechococcus*, which are continuously grazed by rapidly growing microzooplankton (12, 13). In contrast, waters over the continental shelf are rich in iron and silicic acid and support a high biomass of mainly large centric diatoms (14) whose productivity is seasonally limited by nitrogen availability (15). Large-scale current patterns in the Northeast Pacific, combined with estuarine circulation along the coast, introduce a steady supply of relatively fresh coastal water into the more saline oceanic waters (16). The transition zone between the open-ocean and coastal water masses is demarcated at the shelf break by a seasonally persistent gradient in nutrients, salinity, and density (17–19), creating a boundary between the oceanic and coastal phytoplankton communities and potentially a marine ecotone (20).

For over 50 y, hydrographic data have been collected along the Line P transect [extending 1,500 km offshore from the coast of British Columbia, Canada, to Ocean Station Papa (50°N, 145°W)], representing one of the longest oceanographic time series. These time series observations suggest that high productivity exists within the coastal–oceanic transition zone of the Northeast Pacific Ocean, based on the low partial pressure of CO_2 and near complete depletion of nutrients such as nitrate and silicic acid in spring and summer (18, 21, 22) (characteristics associated with phytoplankton growth) within a 100-km–wide salinity gradient off the shelf break (17, 18). Strong gradients in chlorophyll *a* concentrations are also observed across the coastal–oceanic transition zone but there is no detailed information available on the species composition or ecological dynamics of phytoplankton assemblages across this productivity gradient. We developed a flow-through cytometer that allowed us to generate continuous measurements of phytoplankton cell abundance and composition across the intersection of the iron-poor, high-nitrate offshore waters with the iron-rich, low-nitrate coastal waters. Here, we describe natural, iron-fertilized phytoplankton blooms that occur specifically within the transition zone and appear to contribute disproportionately to the biogeochemistry of the region.

Results and Discussion

Phytoplankton Biomass in the Transition Zone. Satellite-based chlorophyll *a* concentrations (Sea-Viewing Wide Field-of-View Sensor, SeaWiFS) indicate that the highest phytoplankton bio-

Author contributions: F.R., A.M., and E.V.A. designed research; F.R., A.M., K.A.H., K.B., C.A.D., R.M., M.R., and J.E.S. performed research; J.E.S., P.D.T., and G.A. contributed new reagents/analytic tools; F.R., A.M., K.A.H., K.B., C.A.D., R.M., M.R., and P.D.T. analyzed data; and F.R., A.M., and E.V.A. wrote the paper.

The authors declare no conflict of interest.

This article is a PNAS Direct Submission.

[1]To whom correspondence should be addressed. E-mail: armbrust@u.washington.edu.

This article contains supporting information online at www.pnas.org/lookup/suppl/doi:10.1073/pnas.1005638107/-/DCSupplemental.

Downloaded by guest on May 13, 2021

ECOLOGY

mass in the eastern subarctic Pacific Ocean in June 2008 occurred along the coast, with intermediate levels around the continental shelf break (Fig. 1*A*). Along the Line P transect in June 2008, coastal waters (from 125 to 126°W) were characterized by a shallow mixed layer (7.6 ± 1.0 m) and high fluorescence-based chlorophyll *a* concentrations (8.8 ± 5.6 μg L^{-1}), resulting in relatively low concentrations of the macronutrients required by phytoplankton—nitrate (2.2 μmol L^{-1}), phosphate (0.4 μmol L^{-1}), and silicic acid (5.6 μmol L^{-1}) at station P1 (Fig. 1*B*). As observed previously (14, 23), the coastal phytoplankton assemblage was dominated by large phytoplankton cells (>50 μm) including centric diatoms such as *Chaetoceros* spp. and *Thalassosira* spp. In contrast, the open ocean phytoplankton community (from 128 to 136°W) was dominated by cells less than 5 μm in size, such as the cyanobacteria *Synechococcus* spp., with low chlorophyll *a* levels (0.3 ± 0.1 μg L^{-1}) and high concentrations of nitrate (8.3 ± 2.3 μmol L^{-1}), phosphate (0.9 ± 0.1 μmol L^{-1}), and silicic acid (10.5 ± 2.1 μmol L^{-1}). In these open ocean waters, iron concentrations were below 0.04 ± 0.01 nmol L^{-1} (Table S1) and growth of the phytoplankton assemblages was likely limited by iron availability.

In June 2008, a steep decrease of partial pressures of CO_2 was observed in surface waters across the continental shelf, with waters supersaturated for CO_2 (477 μatm) relative to the atmosphere (379 μatm) near shore (east of station P1) to CO_2 undersaturated waters (129 μatm) at the shelf break (126°W) (Fig. 1*B*). Coastal upwelling brings CO_2 supersaturated waters to the surface near shore making this part of the coastal zone inefficient at drawing down CO_2 from the atmosphere despite the high phytoplankton biomass (Fig. S1). Further offshore at the shelf break and outside the influence of upwelling, surface waters were undersaturated for CO_2 (Fig. 1*B*). In the open ocean, where phytoplankton biomass was low, pCO_2 in surface waters remained near saturation value (Fig. 1*B*).

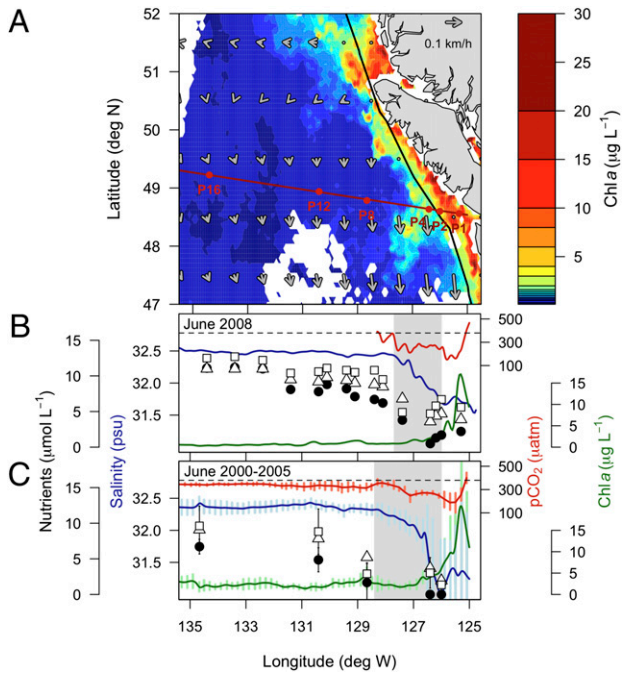

Fig. 1. Hydrographic features of surface waters in the Northeast Pacific Ocean. (*A*) Chlorophyll *a* concentrations and surface currents (arrows) in June 2008. The bathymetry at the shelf break (200 m depth) is represented by the black line, the first half of the Line P transect and location of the six stations (P1, P2, P4, P8, P12, and P16) are indicated in red. (*B* and *C*) Surface concentrations of nitrate (black circle), silicic acid (open square), and 10× phosphate (open triangle) at different stations, and underway measurements of surface seawater salinity (blue line), chlorophyll *a* concentrations (green line), and partial pressure of CO_2 (red line) along the Line P transect (*B*) in June 2008 and (*C*) in June 2000–2005 (seasonal mean based on Line P cruises conducted in June 2000, 2002, 2003, and 2005). The dashed line represents mean atmospheric pCO_2. The blue, green, red, and black error bars in *C* represent the SD of seasonal salinity, chlorophyll *a* concentrations, pCO_2, and nutrient concentrations, respectively. The light gray bar in *B* and *C* highlights the transition zone defined as a change of salinity of ≥0.2 per degree longitude.

The transition zone between coastal and more saline oceanic waters, indicated by the steep increase in salinity (≥0.2 per degree longitude), began immediately west of the continental shelf break (126°W) and spanned ~140 km to 127.7°W in June 2008 (Fig. 1*B*). Surface waters within the transition zone were characterized by a shallow mixed layer (7.2 ± 1.8 m) and fluorescence-based chlorophyll *a* concentrations (1.6 ± 0.6 μg L^{-1}) that were 5.5-fold lower than the neighboring coastal waters (Fig. 1*B*); cells <5 μm in size accounted for 65 and 70% of the total chlorophyll *a* at stations P2 and P4, respectively (Table S1). The mean pCO_2 in surface waters across the transition zone was low (269 ± 34 μatm) relative to the open ocean (359 ± 14 μatm), and only slightly higher than the coastal region (238 ± 93 μatm), indicating a significant impact of the transition zone on uptake of atmospheric CO_2 in the region. When extrapolated to the entire transect (from station P1 to P16), the transition zone accounts for 46% of total atmospheric CO_2 uptake despite only accounting for 20% of the area (Table S2).

Depletion of nutrients and low pCO_2 in surface waters associated with relatively low chlorophyll *a* concentrations is a common feature of the transition zone along Line P in June (Fig. 1*C*). The linear relationship between temperature and salinity (Fig. S2*A*) and the apparent lack of an upwelling signal in the transition zone (Fig. S1) suggest that surface waters in the region are dominated by the mixing of a single coastal water mass with offshore waters. Given the linear gradient of mixing of coastal and offshore waters (Figs. S2*B* and S3*A*), nitrate and silicic acid concentrations at station P4 in June 2008 were fivefold lower than those predicted, based solely on the mixing of the two water types (Fig. S3*B*). This apparent nutrient drawdown is inferred to result form phytoplankton growth. Redfield stoichiometry in nutrient utilization predicts that the phytoplankton biomass resulting from the nutrient drawdown at station P4 was equivalent to the production of 254 ± 41 μg C L^{-1}. Based on a chlorophyll *a* concentration of 1.5 ± 0.1 μg L^{-1} at station P4, the apparent C:Chl *a* ratio was 165 g g^{-1}, which is about two to three times higher than C:Chl *a* ratios commonly used to derive phytoplankton biomass based on chlorophyll *a* concentrations from satellite data (50–90 g C g Chl^{-1}) (24). If our phytoplankton biomass estimate is correct, satellite-based chlorophyll *a* measurements would underestimate phytoplankton biomass, and thus carbon drawdown, within the transition zone.

Small-Celled Phytoplankton Bloom in the Transition Zone. Continuous underway measurements of phytoplankton cell abundance and composition along Line P were made using a custom-built flow-through cytometer that utilizes light scattering and cellular autofluorescence properties of individual cells (25) to discriminate and quantify different phytoplankton populations that span 1–10 μm in nominal cell size (Fig. S4 *A* and *B*). Results from this instrument were in excellent agreement with discrete samples analyzed by conventional flow cytometry (Fig. S4*C*). The cumulative chlorophyll *a* fluorescence derived from cytometry measurements was consistent with the total chlorophyll *a* concentrations measured across the transition and offshore regions. This indicates that the phytoplankton community in these two regions was dominated by cells 1–10 μm in nominal size (Fig. 2*A*), in agreement with size-fractioned chlorophyll *a* measurements at stations P2 and P4 (Table S1).

Downloaded by guest on May 13, 2021

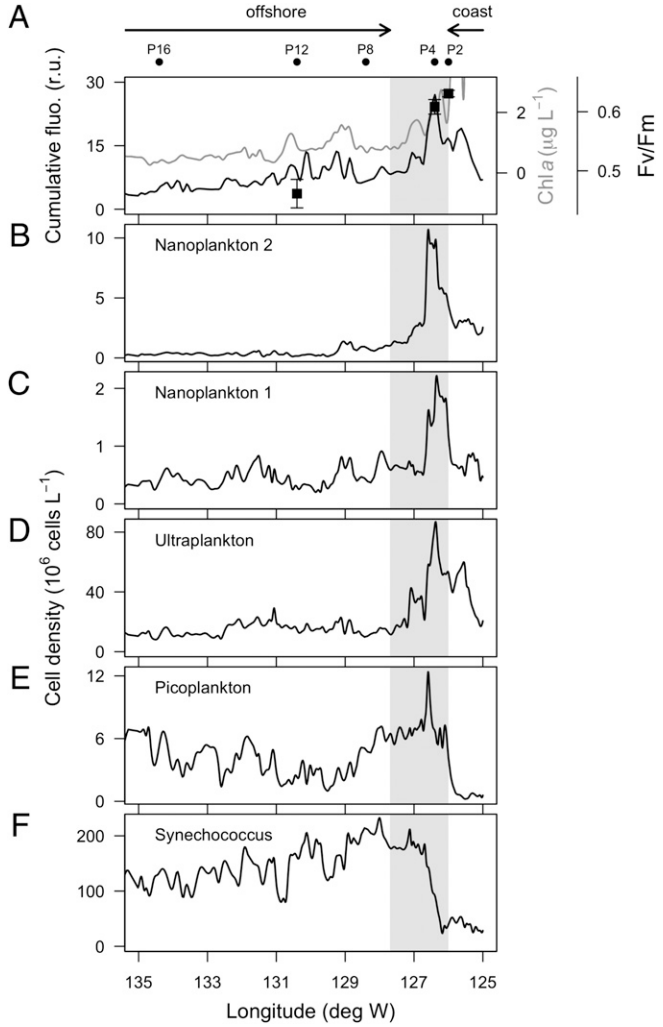

Fig. 2. Chlorophyll *a* fluorescence and spatial distributions of 1- to 10-μm–sized phytoplankton along Line P from May 31 to June 9, 2008. (*A*) Station location (P2, P4, P8, P12, and P16), chlorophyll *a* concentrations (gray line), cumulative fluorescence of the individual phytoplankton cells (black line), and the photosynthetic efficiency F_v/F_m (black square). The two chlorophyll *a* measures are offset to facilitate visualization. (*B–F*) Cell concentrations of five size classes of phytoplankton populations, nanoplankton 1 and 2 (~5 and 7 μm nominal mean cell size, respectively), ultraplankton (~3 μm nominal mean cell size), picoplankton (~2 μm nominal mean cell size), and phycoerythrin-containing *Synechococcus* (~2 μm nominal mean cell size) were measured continuously by flow-through cytometry. The gray bar in each panel highlights the transition zone defined as a change of salinity of ≥0.2 per degree longitude.

A striking succession of blooms of distinct phytoplankton populations was apparent across the transition zone. An abrupt fivefold increase in cell concentrations of two nanoplankton populations (5 and 7 μm nominal mean cell size, respectively) along with a twofold increase in an ultraplankton population (3 μm nominal mean cell size) was observed within a 50-km–wide window on the eastern (coastal) side of the transition zone, with peak abundances at 126.4°W (Fig. 2 *B–D*). High photochemical efficiency of phytoplankton photosystem II (F_v/F_m) at discrete stations in the transition zone (Fig. 2*A*), along with relatively high chlorophyll *a* fluorescence per cell of these three populations (Fig. S5), supports the nutrient-based evidence that cells were actively growing in this region (26). The abundance of ultra- and nanoplankton 1 and 2 populations decreased in the western (oceanic) part of the transition zone, followed by a rapid increase in cell concentrations of the picoplankton and cyanobacteria *Synechococcus* populations (2 μm nominal mean cell size), which remained relatively high within offshore waters (Fig. 2 *E* and *F*). To achieve the same phytoplankton population resolution we observed, a frequency of one discrete sample every 10 min would have been required, which is higher than most oceanographic surveys (Fig. S6).

Assuming that the diversity of phytoplankton cell size and chlorophyll *a* fluorescence measured by flow cytometry indicate richness in physiological and genetic variations (27, 28), the greatest diversity of phytoplankton was observed in the transition zone between station P2 and P4, coinciding with the highest concentrations of ultraplankton and nanoplankton 1 and 2 populations (Fig. S7). Based on cell concentrations and a size-specific cell volume to cell carbon conversion factor (29), we estimate that phytoplankton biomass for cells spanning 1–10 μm in nominal size represent 223 ± 76 μg C L^{-1} throughout the transition zone, with 305 ± 65 μg C L^{-1} at station P4. This value is in close agreement with our biomass estimate of 254 ± 41 μg L^{-1}, which was based on nutrient drawdown estimates (Fig. S3). Thus, consistent with terrestrial ecotones, relatively high species diversity and abundance is found within this confined oceanic region.

Oceanic Phytoplankton Species Dominate the Transition Zone. Phytoplankton species that bloom in the transition zone could be derived from either coastal or oceanic communities, or a combination of both. Measured dissolved iron concentrations were about fivefold higher at station P4 (0.2 ± 0.05 nmol L^{-1}) than the offshore station P12 (0.04 ± 0.01 nmol L^{-1}) (Table S1), suggesting a strong gradient in iron availability across the transition zone (30). Therefore the formation of transition zone phytoplankton blooms could be induced by the shoreward increase in iron concentrations. To address whether iron enrichment of offshore phytoplankton communities created blooms comparable to those occurring within the transition zone, a microcosm iron-enrichment experiment was performed at Station Papa (P26), a well-characterized iron-limited region (10, 31). Experimental iron enrichment induced a temporal succession of small-celled phytoplankton blooms that was strikingly similar to the succession of species observed across the transition zone. Iron enrichment caused the ambient *Synechococcus*-dominated assemblage at Station Papa to shift to an ultra- and nanoplankton 1 and 2 population-dominated assemblage within 4 d (Fig. 3*A*), consistent with previous observations in the Northeast Pacific Ocean (32). The species composition of the pennate diatom *Pseudo-nitzschia* that dominated the nanoplankton 2 population at Station Papa after addition of iron was similar to *Pseudo-nitzschia* species composition at stations P2 and P4 in the transition zone, including the species *Pseudo-nitzschia granii*, which is classified as primarily oceanic (33) (Fig. 3 *B* and *C*). Note that due to their long and narrow cell type (from 21 to 88 μm in length and from 1.4 to 5.1 μm in diameter) (34), pennate diatoms such as *Pseudo-nitzschia* have a low light scattering relative to their cell sizes and therefore are categorized as nanoplankton populations (from 5 to 20 μm) by flow cytometry (25) rather than their conventional classification as microplankton (>20 μm) based on microscopy. These results indicate that the phytoplankton composition within the transition zone is consistent with an iron-enriched offshore community rather than a nitrate-enriched coastal community. The high abundances of small-celled phytoplankton appear to have resulted from a natural iron enrichment of open ocean waters being transported toward iron-rich coastal waters. Although, it should be noted that the community responses to iron enrichment is expected to vary depending on the location of the transition zone along the Line P transect (20).

Two possible scenarios could explain the observed succession of phytoplankton populations within the ecotone. In the first scenario, the blooms are driven by spatial gradients in iron: macronutrient availability, with nutrient ratios increasing linearly

Downloaded by guest on May 13, 2021

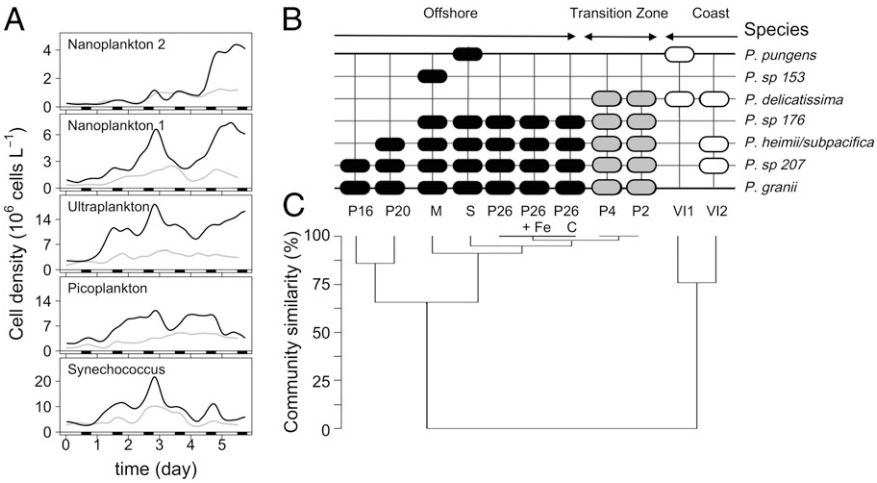

Fig. 3. Temporal distribution of five phytoplankton populations following artificial iron enrichment of HNLC waters and *Pseudo-nitzschia* distributions along Line P. (*A*) Cell concentrations of five size classes of phytoplankton populations, nanoplankton 1 and 2 (~5 and 7 μm nominal mean cell size, respectively), ultraplankton (~3 μm nominal mean cell size), picoplankton (~2 μm nominal mean cell size), and *Synechococcus* (~2 μm nominal mean cell size) were measured continuously with flow-through cytometry in an unamended control (gray line) and after addition of 4 nM of $FeCl_3$ (black line). For clarity, data were fitted with a cubic polynomial regression model. The black bars indicate night. (*B* and *C*) Comparisons of the pennate diatom *Pseudo-nitzschia* species assemblages along offshore, transition zone and coastal stations. Previously published ARISA profiles from the SERIES experiment (S represents the in situ iron-enriched patch on day 18, M represents an on-deck iron incubation at day 11, July 2002) (33) and from coastal waters of Vancouver Island (VI1 from Tofino Inlet, August 2004 and VI2 from outside Esperanza Inlet, August 2005) (50) were included in the analysis to show that *Pseudo-nitzschia* species distributions across the transition zone were more similar to the open-ocean in situ iron enrichment than to coastal waters. Species detected along Line P included *P. pungens, P. delicatissima, P. heimii/subpacifica*, and *P. granii* as well as *P.* sp 153, *P.* sp 176, and *P.* sp 207 that could not be identified to the species level. (*B*) The presence or absence of *Pseudo-nitzschia* species among the coastal water stations (VI1 and VI2) (white rounded rectangle), transition zone stations (P2 and P4) (gray rounded rectangle), and offshore stations (P16, P20, and P26) and iron-enrichment experiments (S, M, and P26 control and P26 + Fe 96 h after enrichment) (black rounded rectangle); additional species were detected in coastal waters (50), but only those shared with transition zone or offshore waters are shown. (*C*) Pairwise similarity comparisons of *Pseudo-nitzschia* species assemblages at different stations.

toward the coast. This explanation assumes that the size dependence of nutrient requirements, uptake and growth (35), dictate where individual species bloom within the ecotone. In this scenario, small-celled phytoplankton, which have lower cellular iron requirements than large cells (36), would bloom on the oceanic side of the transition zone, whereas large-celled phytoplankton such as diatoms would bloom in the coastal side of the transition zone. An alternative scenario is that succession of phytoplankton populations is determined by the length of time since the open ocean community was first exposed to higher iron as it moves toward the coast. This explanation assumes that iron fertilization starts at the oceanic side of the transition zone (time 0) and that a combination of seed population size and net growth rates dictate the amount of time required for individual species to bloom. This is analogous to our incubation enrichment at Station Papa (Fig. 3*A*) or to the previous iron-enrichment experiment in the Northeast Pacific Ocean (32). In this scenario, small-celled phytoplankton would dominate during the early stage of the bloom (i.e., oceanic side of the transition zone) because of their relatively higher seed populations size and higher growth rate than large cells. These small cells would then be progressively held in check in the later stage of the bloom (i.e., coastal side of the transition zone) as the numbers of microzooplankton grazing increased, while large cells would eventually reach high abundances and dominate because of their reduced susceptibility to micrograzers. Under near steady-state conditions where the mixing of the iron-rich coastal waters with HNLC waters is constant, both scenarios would result in comparable partitioning of ecological niche space and enhancement of phytoplankton diversity and productivity across the ecotone. The extent to which these blooms act to sequester carbon will depend upon their capacity to sink into the deep ocean, which is primarily driven by their production rates, the size of the cells, and their tendency to form aggregates (37).

Concluding Remarks. This study describes blooms of small-celled phytoplankton in a narrow but seasonally persistent environmental gradient at the intersection of iron-poor, nitrate-rich offshore waters and iron-rich, nitrate-poor coastal waters in the Northeast Pacific Ocean. These blooms are characterized by high species diversity and appear to result from a natural iron fertilization of oceanic species, including the pennate diatom *P. granii*, that possesses intrinsically low iron requirements and can presumably outcompete coastal species that have much higher iron requirements (38). Depletion of nutrients and low pCO_2 in surface waters associated with relatively low chlorophyll *a* concentrations is recurrently observed in the transition zone, suggesting that these small-celled blooms are a common feature of this specialized region with a disproportionate impact on nutrient and atmospheric CO_2 drawdown. The transition zone is expected to expand and contract over seasonal cycles due to changes in ocean circulation (21). The ability to detect and track these small-celled blooms is therefore critical for understanding the biogeochemical impact of this important yet poorly characterized oceanic region.

Diverse and complex phytoplankton blooms, such as those described in this study, are characteristic features of ecotones (1) and are likely to flourish in steep physical gradients throughout the world's oceans, particularly in regions where water masses with complementary nutrient compositions mix. For example, oceanic fronts between distinct water masses in HNLC regions are commonly associated with high species diversity and productivity (4, 39, 40). Physiologically and genetically diverse groups of organisms confer the ability to adapt to abrupt changes in environmental conditions. Therefore, similar to terrestrial ecosystems (41), changes in production and composition at ecotones may serve as an early indicator of climate-change impacts.

Materials and Methods

Underway Measurements. In June 2008, subsurface seawater from the vessel seawater supply (intake at 4.5 m depth) was sampled for continuous un-

Downloaded by guest on May 13, 2021

derway measurements of salinity, temperature, and fluorescence by thermosalinograph fluorometry, pCO_2 by membrane inlet mass spectrometry (MIMS) (42), and phytoplankton cell abundances and cellular autofluorescence by a custom-built flow-through cytometer (*SI Materials and Methods*) (43). Data available from the Line P program were used to calculate the seasonal mean of salinity, chlorophyll *a* concentration (June 2000, 2002, 2003, and 2005) (http://www.pac.dfo-mpo.gc.ca/) and pCO_2 (2002 and 2003) (http://cdiac.ornl.gov/).

Satellite Data. Chlorophyll *a* concentrations were obtained from SeaWiFS data (http://disc.sci.gsfc.nasa.gov); surface currents velocity and direction were derived from surface topography (Jason-1 altimeter), vector winds (Quick Scatterometer), and sea surface temperature (MODIS) data obtained from JPL Physical Oceanography DAAC and developed by Earth and Space Research (http://www.oscar.noaa.gov/) (44).

Hydrographical Data. In June 2008, discrete, size-fractioned chlorophyll *a* concentrations were determined by the in vitro fluorometry using the acidification method (45). Seawater samples (400 mL) were filtered sequentially through a 5-μm pore-size polycarbonate filter and a GF/F filter (0.7 μm nominal pore size) using a filter cascade. Maximum photochemical yields of photosystem II (PSII) (F_v/F_m) were performed on water samples using a Phyto-PAM fluorometer (Walz). Before each measurement, a subsample (5 mL) of water was placed in the dark for 20 min. The constant fluorescence of dark-acclimated phytoplankton (F_o) was measured using modulated light at a low intensity (11 μmol quanta m^{-2} s^{-1}) to avoid the reduction of the photosystem II primary electron acceptors. The maximal fluorescence yield (F_m) was induced by a short (200 ms), saturating pulse of light (3,500 μmol quanta m^{-2} s^{-1}), which triggered the reduction of all PSII plastoquinone pools. F_v/F_m was calculated as described in Schreiber et al. (46) after the subtraction of a 0.2-μm filtered seawater blank.

Samples for nitrate, phosphoru,s and silicic acid were collected at discrete stations using Niskin bottles mounted onto a rosette system and measured on an Astoria autoanalyzer. Data from the Line P program were used to calculate the seasonal mean of nutrient concentrations (2000–2005) (http://www.pac.dfo-mpo.gc.ca/). For measurements of dissolved iron (DFe) concentrations, 0.22-μm filtered seawater sampled at 0, 10, 20, 30, and 40 m depth was collected in acid-washed 250-mL low-density polyethylene bottles and buffered to pH 3.5 for 1–2 h before FIA chemiluminescent analysis following the method of Obata et al. (47, 48). Iron concentrations represent the average value of the five depth samples. More details of the method, processing, and definitions of iron fractions can be found in Johnson et al. (49).

Underway Flow Cytometer. The instrument was modified from an Influx high-speed cell sorter (BD Biosciences) to include the position-sensitive detector (PSD) system (43). Details of the electronics, optics, and fluidics of instrument are provided in *SI Materials and Methods*. The volume of seawater analyzed by the instrument flow rate was set up at ~94 μL min^{-1} along the transect to sample the highest volume without coincidence error, and ~50 μL min^{-1} during the iron-enrichment microcosm experiment to sample continuously for at least 6 d. Data files were created every 10 min and analyzed using FlowJo version 8.8 (Tree Star). Optimally positioned particles were identified by normalizing the signal of the position-sensitive detector by the forward angle light scatter signal (collected using a 480–10 bandpass filter) (43). Phycoerythrin (PE)-positive cells (*Synechococcus*) and PE-negative cells (all other phytoplankton) were classified on the basis of orange fluorescence (collected using a 572–27 bandpass filter). Light scattering and red fluorescence (collected using a 480–10 bandpass filter) were used to distinguish four populations within PE-negative cells, namely "picoplankton," "ultraplankton," "nanoplankton 1," and "nanoplankton 2." Discrete samples for cytometry analysis were taken every 6 h directly from the outflow of the flow-through cytometer, fixed with 1% paraformaldehyde and 0.01% glutaraldehyde, and frozen in liquid nitrogen, and analyzed onshore by an Influx high-speed cell sorter (BD Biosciences) for comparison.

Iron-Enrichment Microcosm Experiment. Unfiltered seawater from 10 m depth was transferred to two 50-L acid-cleaned low-density polyethylene (LDPE) carboys with Teflon-lined tubing and a Teflon bellows pump within a trace metal clean laminar flow hood. One bottle was enriched with 4 nM $FeCl_3$ and the other served as an unamended control. Bottles were incubated on deck in Plexiglas incubators wrapped in neutral density screening to achieve 30% incident irradiance and were maintained at near ambient sea surface temperature using a seawater flow-through system. Both bottles were connected by polyvinyl chloride (PVC) tubing (Tygon Biocompatible S-50-HL) directly to the cytometer and sampled alternatively every 15 min using a peristaltic pump.

***Pseudo-nitzschia* Species Identification.** DNA was extracted from 10-L surface water samples (collected with the rosette system) and the incubation samples using the DNeasy Plant mini kit (Qiagen). Triplicate PCRs for automated ribosomal intergenic spacer analysis (ARISA) were performed for each sample, using primers designed to recognize a fragment from the ITS1 region of *Pseudo-nitzschia* species (50). Pairwise similarity comparisons of *Pseudo-nitzschia* assemblages were conducted in PRIMER-E (51) using Jaccard's similarity index in conjunction with the group average algorithm for clustering analysis.

ACKNOWLEDGMENTS. We thank the scientists of Fisheries and Oceans Canada at the Institute of Ocean Sciences (IOS), Sidney, BC, and the officers and crew aboard the Canadian Coast Guard Ship John P. Tully for their assistance during the cruise. We are grateful to S. Johannessen, J. Barwell-Clarke, and K. Johnson (Institute of Ocean Science, Sidney, BC, Canada) for sharing pCO_2, nutrients, and iron data, respectively; A. Bailey for helping with ARISA profiles; and P. J. Harrison and S. N. Coesel for comments on an earlier version of the manuscript. This study was supported by a Gordon and Betty Moore Foundation Marine Microbiology Investigator Award, National Science Foundation grants, a National Institute of Environmental Health Sciences grant, and a National Oceanic and Atmospheric Administration training grant (to E.V.A).

1. Longhurst A (1998) *Ecological Geography of the Sea* (Academic Press, San Diego).
2. Holland M, Risser PG, Naiman RJ (1991) *Ecotones: The Role of Landscape Boundaries in the Management and Restoration of Changing Environments* (Chapman and Hall, London).
3. Smith TB, Wayne RK, Girman DJ, Bruford MW (1997) A role for ecotones in generating rainforest biodiversity. *Science* 276:1855–1857.
4. Barton AD, Dutkiewicz S, Flierl G, Bragg J, Follows MJ (2010) Patterns of diversity in marine phytoplankton. *Science* 327:1509–1511.
5. Springer AM, McRoy CP, Flint MV (1996) The Bering Sea Green Belt: Shelf-edge processes and ecosystem production. *Fish Oceanogr* 5:205–223.
6. Crawford WR, Brickley PJ, Peterson TD, Thomas AC (2005) Impact of Haida eddies on chlorophyll distribution in the eastern Gulf of Alaska. *Deep Sea Res Part II Top Stud Oceanogr* 52:975–989.
7. Crawford WR, Brickley PJ, Thomas AC (2007) Mesoscale eddies dominate surface phytoplankton in northern Gulf of Alaska. *Prog Oceanogr* 75:287–303.
8. Okkonen SR, Schmidt GM, Cokelet ED, Stabeno PJ (2004) Satellite and hydrographic observations of the Bering Sea 'Green Belt'. *Deep Sea Res Part II Top Stud Oceanogr* 51:1033–1051.
9. Takahashi T, et al. (2002) Global sea-air CO_2 flux based on climatological surface ocean pCO2, and seasonal biological and temperature effects. *Deep Sea Res Part II Top Stud Oceanogr* 49:1601–1622.
10. Boyd PW, et al. (2004) The decline and fate of an iron-induced subarctic phytoplankton bloom. *Nature* 428:549–553.
11. Harrison PJ, et al. (1999) Comparison of factors controlling phytoplankton productivity in the NE and NW subarctic Pacific gyres. *Prog Oceanogr* 43:205–234.
12. Miller CB, et al. (1991) Ecological dynamics in the Subarctic Pacific, a possibly iron-limited ecosystem. *Limnol Oceanogr* 36:1600–1615.
13. Frost BW (1991) The role of grazing in nutrient-rich areas of the open Sea. *Limnol Oceanogr* 36:1616–1630.
14. Taylor FJR, Haigh R (1996) Spatial and temporal distributions of microplankton during the summers of 1992-1993 in Barkley Sound, British Columbia, with emphasis on harmful species. *Can J Fish Aquat Sci* 53:2310–2322.
15. Harris SL, Varela DE, Whitney FW, Harrison PJ (2009) Nutrient and phytoplankton dynamics off the west coast of Vancouver Island during the 1997/98 ENSO event. *Deep Sea Res Part II Top Stud Oceanogr* 56:2487–2502.
16. Whitney FA, Crawford WR, Harrison PJ (2005) Physical processes that enhance nutrient transport and primary productivity in the coastal and open ocean of the subarctic NE Pacific. *Deep Sea Res Part II Top Stud Oceanogr* 52:681–706.
17. Favorite F, Dodimead AJ, Nasu K (1976) Oceanography of the subarctic Pacific region, 1960-1971. *Int North Pac Fish Comm Bull* 33:1–187.
18. Whitney FA, Wong CS, Boyd PW (1998) Interannual variability in nitrate supply to surface waters of the Northeast Pacific Ocean. *Mar Ecol Prog Ser* 170:15–23.
19. Cullen JT, Chong M, Ianson D (2009) British Columbian continental shelf as a source of dissolved iron to the subarctic northeast Pacific Ocean. *Global Biogeochem Cycles* 23: GB4012.
20. Boyd P, Berges JA, Harrison PJ (1998) In vitro iron enrichment experiments at iron-rich and -poor sites in the NE subarctic Pacific. *J Exp Mar Biol Ecol* 227:133–151.
21. Whitney FA, Freeland HJ (1999) Variability in upper-ocean water properties in the NE Pacific Ocean. *Deep Sea Res Part II Top Stud Oceanogr* 46:2351–2370.
22. Nemcek N, Ianson D, Tortell PD (2008) A high-resolution survey of DMS, CO_2, and O_2/Ar distributions in productive coastal waters. *Global Biogeochem Cycles* 22:GB2009.
23. Perry RI, Dilke BR, Parsons TR (1983) Tidal mixing and summer plankton distributions in Hecate Strait, British-Columbia. *Can J Fish Aquat Sci* 40:871–887.

Downloaded by guest on May 13, 2021

24. Behrenfeld MJ, Boss E, Siegel DA, Shea DM (2005) Carbon-based ocean productivity and phytoplankton physiology from space. *Global Biogeochem Cycles* 19:GB1006.
25. Olson RJ, Zettler ER, Anderson OK (1989) Discrimination of eukaryotic phytoplankton cell types from light scatter and autofluorescence properties measured by flow cytometry. *Cytometry* 10:636–643.
26. Geider R, Roche J (1994) The role of iron in phytoplankton photosynthesis, and the potential for iron-limitation of primary productivity in the sea. *Photosynth Res* 39: 275–301.
27. Li WKW (1997) Cytometric diversity in marine ultraphytoplankton. *Limnol Oceanogr* 42:874–880.
28. Li WKW (2002) Macroecological patterns of phytoplankton in the northwestern North Atlantic Ocean. *Nature* 419:154–157.
29. Montagnes DJS, Berges JA, Harrison PJ, Taylor FJR (1994) Estimating carbon, nitrogen, protein, and chlorophyll a from volume in marine phytoplankton. *Limnol Oceanogr* 39:1044–1060.
30. La Roche J, Boyd PW, McKay RML, Geider RJ (1996) Flavodoxin as an in situ marker for iron stress in phytoplankton. *Nature* 382:802–805.
31. Martin JH, Fitzwater SE (1988) Iron deficiency limits phytoplankton growth in the north-east Pacific subarctic. *Nature* 331:341–343.
32. Marchetti A, et al. (2006) Phytoplankton processes during a mesoscale iron enrichment in the NE subarctic Pacific: Part I–Biomass and assemblage. *Deep Sea Res Part II Top Stud Oceanogr* 53:2095–2113.
33. Marchetti A, et al. (2008) Identification and assessment of domoic acid production in oceanic *Pseudo-nitzschia* (Bacillariophyceae) from iron-limited waters in the Northeast Subarctic Pacific. *J Phycol* 44:650–661.
34. Marchetti A, Harrison PJ (2007) Coupled changes in the cell morphology and the elemental (C, N, and Si) composition of the pennate diatom *Pseudo-nitzschia* due to iron deficiency. *Limnol Oceanogr* 52:2270–2284.
35. Eppley RW, Rogers JN, McCarthy JJ (1969) Half-saturation constants for uptake of nitrate and ammonium by marine phytoplankton. *Limnol Oceanogr* 14:912–920.
36. Sunda WG, Huntsman SA (1995) Iron uptake and growth limitation in onceanic and coastal phytoplankton. *Mar Chem* 50:189–206.
37. Richardson TL, Jackson GA (2007) Small phytoplankton and carbon export from the surface ocean. *Science* 315:838–840.
38. Marchetti A, et al. (2009) Ferritin is used for iron storage in bloom-forming marine pennate diatoms. *Nature* 457:467–470.
39. Yoder JA, et al. (1994) A line at sea. *Nature* 371:689–692.
40. Knox GA, ed (2009) *Biology of the Southern Ocean* (CRC Press, Boca Raton, FL), 2nd Ed, p 533.
41. Neilson RP (1993) Transient ecotone response to climatic change: Some conceptual and modelling approaches. *Ecol Appl* 3:385–395.
42. Tortell PD (2005) Dissolved gas measurements in oceanic waters made by membrane inlet mass spectrometry. *Limnol Oceanogr Methods* 3:24–37.
43. Swalwell JE, Petersen TW, van den Engh G (2009) Virtual-core flow cytometry. *Cytometry A* 75A:960–965.
44. Bonjean F, Lagerloef GSE (2002) Diagnostic model and analysis of the surface currents in the tropical Pacific Ocean. *J Phys Oceanogr* 32:2938–2954.
45. Parsons T, Maita Y, Lalli CM (1984) *A Manual of Chemical and Biological Methods for Seawater Analysis* (Pergamon Press, New York).
46. Schreiber U, Schliwa U, Bilger W (1986) Continuous recording of photochemical and non-photochemical chlorophyll fluorescence quenching with a new type of modulation fluorometer. *Photosynth Res* 10:51–62.
47. Obata H, Karatani H, Nakayama E (1993) Automated determination of iron in seawater by chelating resin concentration and chemiluminescence detection. *Anal Chem* 65:1524–1528.
48. Obata H, Karatani H, Matsui M, Nakayama E (1997) Fundamental studies for chemical speciation of iron in seawater with an improved analytical method. *Mar Chem* 56: 97–106.
49. Johnson KW, Miller LA, Sutherland NE, Wong CS (2005) Iron transport by mesoscale Haida eddies in the Gulf of Alaska. *Deep Sea Res Part II Top Stud Oceanogr* 52: 933–953.
50. Hubbard KA, Rocap G, Armbrust EV (2008) Inter- and intraspecific community structure within the diatom genus *Pseudo-nitzschia* (Bacillariophyceae). *J Phycol* 44: 637–649.
51. Clarke KR, Warwick RM (2001) *Primer-E* (Plymouth, UK), p 172.

Downloaded by guest on May 13, 2021